The Astronomical Journal, 130:2262–2271, 2005 November

ADAPTIVE OPTICS PHOTOMETRY AND ASTROMETRY OF BINARY STARS[1]

Lewis C. Roberts, Jr.
The Boeing Company, 535 Lipoa Parkway, Suite 200, Kihei, HI 96753; lewis.c.roberts@boeing.com

Nils H. Turner
CHARA, Georgia State University, Mount Wilson, CA 91023; nils@chara-array.org

L. William Bradford
The Boeing Company, 535 Lipoa Parkway, Suite 200, Kihei, HI 96753; lawrence.w.bradford@boeing.com

Theo A. ten Brummelaar
CHARA, Georgia State University, Mount Wilson, CA 91023; theo@chara-array.org

Ben R. Oppenheimer
Department of Astrophysics, American Museum of Natural History, Central Park West at 79th Street, New York, NY 10024; bro@amnh.org

Jeff R. Kuhn and Kathryn Whitman
Institute for Astronomy, University of Hawaii, 2680 Woodlawn Drive, Honolulu, HI 96822; kuhn@ifa.hawaii.edu, whitman@ifa.hawaii.edu

and

Marshall D. Perrin and James R. Graham
Astronomy Department, University of California, 601 Campbell Hall, Berkeley, CA 94720; mperrin@astron.berkeley.edu, jrg@astron.berkeley.edu
Received 2005 June 7; accepted 2005 July 21

ABSTRACT

We present astrometric and photometric measurements of 39 binary stars made with the adaptive optics system on the 3.6 m Advanced Electro-Optical System (AEOS) telescope, taken from 2002 November to 2003 March. The binaries have separations ranging from 0.″08 to 5.″11 and differential magnitudes ranging from 0.096 to 7.9. Also, we include a list of observations of 23 known binaries that we were unable to resolve. In the process of these measurements, we discovered three new companions to two previously known binary stars. We also discuss the effects of scintillation and anisoplanatism on measurements of binary star photometry in adaptive optics images. Suggestions on how to minimize these effects are then given.

Key words: astrometry — binaries: close — binaries: visual — instrumentation: adaptive optics — techniques: photometric

1. INTRODUCTION

Astrometry of binary stars is one of the oldest branches of observational astronomy. New techniques have continuously been introduced that allow the observation of binary systems with smaller separations and increasing dynamic ranges. One of the latest technologies to be applied to binary stars is adaptive optics (AO). In an AO system, the image-distorting effects of atmospheric turbulence are corrected in real time, producing near–diffraction-limited images.

While using an AO system may appear on the surface to be relatively simple, there are many pitfalls. One of the most vexing problems is measuring photometry from AO images. Esslinger & Edmunds (1998) were some of the first to explore AO photometry. They used a combination of real and simulated data to further the understanding of the issues involved. While this paper was extensive, it did not deal with binary stars. AO observations of binary stars have shown variation in the measured photometry in excess of what is expected from simple noise analysis (ten Brummelaar et al. 1998; Barnaby et al. 2000). In order to better understand photometry taken with AO on binary stars, we observed numerous binary stars systems in late 2002 and early 2003 with the AO system on the 3.63 m Advanced Electro-Optical System (AEOS) telescope (Roberts & Neyman 2002) at the Maui Space Surveillance System in Hawaii. This paper presents what we have learned about AO photometry along with the astrometry and photometry of those systems.

2. AO PHOTOMETRY

As mentioned above, the differential magnitudes measured from a sequence of images of binary stars show variation in excess of what is expected. This behavior has been seen in data taken with a variety of AO systems: the Hooker 100 inch (2.5 m; ten Brummelaar et al. 1998), the Starfire Optical Range (SOR) 1.5 m (Barnaby et al. 2000; Roberts 1998), and the SOR 3.5 m (Barnaby et al. 2000). Figure 1 shows similar behavior with the AEOS AO system for WDS 05480+0627 (STF 795) with a measured separation of 1.″07. The data frames were taken with an *I*-band filter. The exposure times of individual frames was 598 ms, and the data were taken over a period of 5 minutes. The *I*-band differential magnitudes have a mean of 0.409 and a standard deviation of 0.013. Other data sets from the AEOS AO system show similar behavior. These variations are not caused by the

[1] Based on observations made at the Maui Space Surveillance System operated by Detachment 15 of the US Air Force Research Laboratory's Directed Energy Directorate.

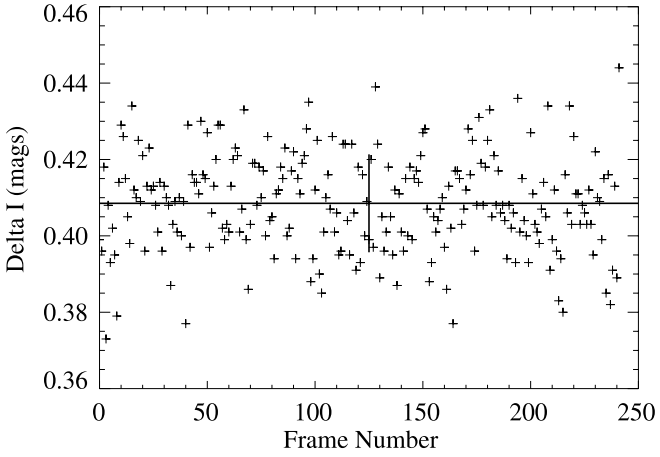

FIG. 1.—Frame-by-frame comparison of the differential magnitudes taken of STF 795 with the AEOS AO system on 2003 January 3. The horizontal line through the data set is the mean magnitude (0.409), while the vertical line is 1 σ (0.013) above and below the mean.

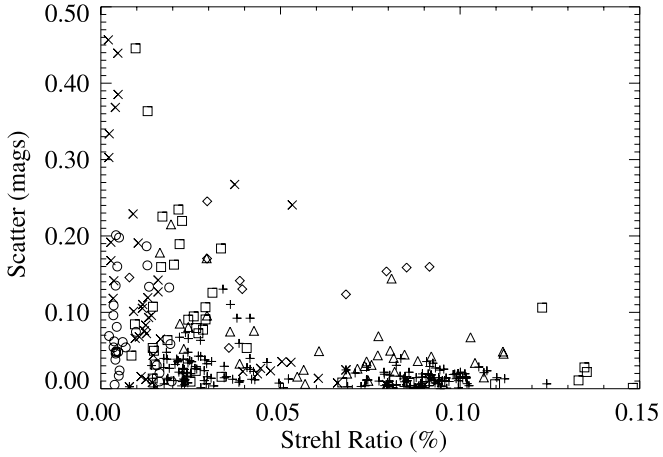

FIG. 2.—Strehl ratio plotted against scatter. Plus signs are for AEOS 700–1060 nm data, asterisks are for SOR *i*-band data, diamonds are for SOR *r*-band data, triangles are for MWI-AO *I*-band data, squares are for MWI-AO *R*-band data, crosses are for MWI-AO *V*-band data, and circles are for MWI-AO *B*-band data.

moment-to-moment point-spread function (PSF) variations that AO systems normally demonstrate. If it was simply the PSF varying, then the peak intensity of both stars would change in the same way, but the relative brightness would remain the same.

In addition to AEOS AO data, we have access to AO data from the 1.5 m telescope at SOR (Fugate et al. 1994) and the Mount Wilson Institute AO (MWI-AO) natural guide star system at the 100 inch telescope at Mount Wilson (Shelton et al. 1995). These data were previously published in ten Brummelaar et al. (1996; 1998). All the observed stars have been measured routinely using speckle interferometry and have separations of approximately 0.″5. The stars that we will analyze in this section are all F stars and hence have similar colors. Details of the individual star systems are given in Table 1.

The observational scheme was the same with all three AO systems: many frames were taken sequentially. Each frame is exposed until just before the CCD enters the nonlinear regime; this way the signal-to-noise ratio (S/N) can be improved by adding many frames together. Due to the different telescope diameters, detectors, and filters used in each system, the images have a range of exposure times. Most of the exposure times were less than 0.5 s, although the MWI-AO data taken in *B*-band and *V*-band exposure times varied from 0.5 to 5 s. The MWI-AO system and the SOR camera were both 16 bit cameras, while the AEOS CCD is a 12 bit detector and has shorter exposure times to avoid saturation.

Multiple filters are used to provide a more complete picture of each binary. At SOR the observations were done with two filters with central wavelengths of 798 nm with a FWHM of 108 nm and 884 nm with a FWHM of 122 nm. These filters were designated *r* and *i*. The Mount Wilson observations were done in the standard Bessel *B*, *V*, *R*, and *I* filters. This set of AEOS observations was taken with a filter with a bandpass of 700–1060 nm. Once the AO data were collected, the individual frames were debiased and flat-fielded. The astrometry and photometry of the binary star were extracted from the AO image using the iterative blind deconvolution algorithm, *fitstars*, described in ten Brummelaar et al. (2000). The only substantive change to the algorithm is that it now works on multiple star systems.

In Figure 2 we plot the scatter versus the Strehl ratio. The Strehl ratio is the ratio of the maximum intensity of the image to the maximum intensity of a perfect diffraction-limited image (Strehl 1901). The scatter, *S*, was defined as

$$S = \left|\overline{\Delta m} - \Delta m_i\right|, \quad (1)$$

where $\overline{\Delta m}$ is the average differential magnitude for an entire data set of a given star, and Δm_i is the differential magnitude from an individual frame. The Strehl ratios were computed with the technique described by Roberts & Neyman (2002). There are several important things to note in this graph. First, the scatter falls with increasing Strehl ratio. Second, measurements from AEOS 700–1060 nm data have much less scatter than the *I*-band data taken from other telescopes. The 700–1060 nm filter is very close to an *I*-band filter.

In order to determine whether the scatter was a data reduction artifact, we created artificial binaries by convolving two point sources with an AO PSF of a single star. For the PSFs, we

TABLE 1

VARIOUS PROPERTIES OF THE BINARY STARS USED IN THE COMPARISON OF SCATTER AS A FUNCTION OF STREHL RATIO

Name	Date	*V* Magnitude	Separation (arcsec)	Spectral Type	AO System	Guide Star
ADS 8804	1995.4	5.2	0.4	F5 V	SOR	Laser
ADS 14073	1995.8	3.6	0.3	F6 IV	SOR	Laser
ADS 14073	1996.5	3.6	0.3	F6 IV	MWI-AO	Natural
ADS 14787	1996.5	3.8	0.8	F2 IV	MWI-AO	Natural
COU 14	1996.5	5.3	0.4	F2 IV	MWI-AO	Natural
COU 14	2000.9	5.3	0.4	F2 IV	AEOS	Natural
ADS 15176	2000.9	6.3	0.5	F7 III	AEOS	Natural

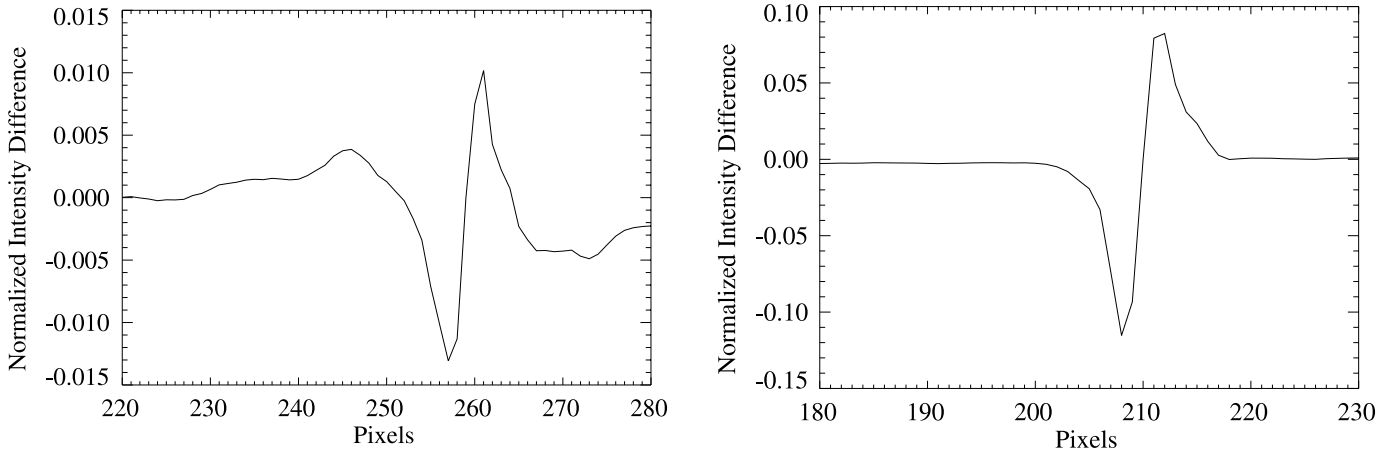

FIG. 3.—Difference between normalized slices taken through the primary and the secondary PSFs. *Left*: STF 346 with a measured separation of 0.″37 and a ΔI of 0.10. *Right*: Results for STF 795 with a measured separation of 1.″08 and a ΔI of 0.41. These plots show that the primary and the secondary PSF do not have the same profile and that the magnitude of the difference changes for each binary star.

selected 100 frames from a number of unresolved systems (see § 4.3 and Table 7 for more details). We used these PSFs to create artificial binaries with varying separations and varying differential magnitudes. Using a collection of 100 frames ensures that we will have a wide variety of PSFs with varying Strehl ratios.

We measured the differential magnitude of these artificial binary frames the same way we measured it for the real binaries. The scatter from the artificial stars was far lower than for real binaries. For instance, an artificial binary was created with the same separation and differential magnitude as STF 795 (the star featured in Fig. 1). While the real data had a standard deviation of 0.013, the artificial binary had a standard deviation of 0.0012, approximately a factor of 10 less. For all cases, the spread in differential magnitude for artificial binaries was a fraction of the spread of real data.

Since the artificial binaries were created by convolving a single PSF with two delta functions, the PSF is identical for each component of the binary. The *fitstars* algorithm assumes that the binary star is composed of two identical PSFs. This implies that the real data does not have identical PSFs. While they look identical to the naked eye, there is a slight difference that changes from frame to frame and causes these variations. We verified this by taking a one-dimensional slice through the image at the location of the primary and the secondary. Each slice was normalized, and the secondary slice was shifted so that its peak was aligned with the primary's peak. The difference between the two slices was computed and is shown in Figure 3 for two stars, STF 346 and STF 795. STF 346 has a measured separation of 0.″37 and a ΔI of 0.10, while STF 795 has a measured separation of 1.″08 and a ΔI of 0.41. This shows the PSFs vary by a small but measurable amount. The question is what causes the slight difference.

Some of the scatter comes from the data analysis technique itself and affects both real and simulated data. The algorithm will have an easier time detecting the secondary when the secondary PSF has a high S/N. If there is a high background, such as the secondary being located in the primary PSF halo, or the secondary PSF is quite faint, then the errors increase.

Another source of errors is that the *fitstars* algorithm models the PSF on a point-by-point basis out to a certain distance. This distance is normally two-thirds of the separation between the primary and secondary. After this point, it assumes the PSF is circularly symmetric. In the case of two well-separated PSFs, *fitstars* models the entire PSF quite well, but in the case in which the two stars are close enough that the PSFs overlap, errors are introduced. So binaries that are widely separated will have their PSFs more accurately measured, and the measured astrometry and photometry will be more accurate. This is demonstrated by Figure 4, in which we plot the standard deviation as a function of differential magnitude for binaries with separations of 0.″5 and 1.″0. The standard deviation increases with increasing differential magnitude and decreasing separation.

This behavior is not isolated to *fitstars*. Christou et al. (2004) compare photometry and astrometric measurements of AO images of a stellar cluster using three different methods. The problem of astrometry and photometry of a cluster is similar to that for a binary star, and at least two of the methods have been used on binary stars (Barnaby et al. 2000). All three methods have errors that change with separation, which is similar to *fitstars*, but the specific shape of the error curve varies. While data reduction methods have an intrinsic scatter, this only accounts for a small part of the observed scatter, so we must consider other causes.

2.1. *Scintillation*

While the data analysis algorithm, *fitstars*, causes some of the scatter, the photometry measured from artificial binaries have

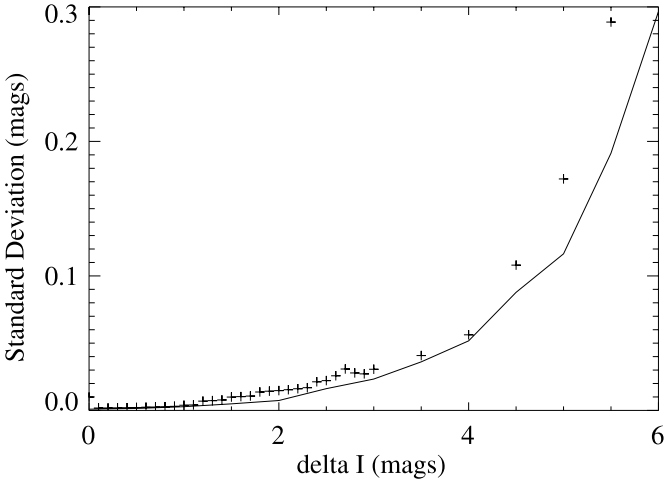

FIG. 4.—Standard deviation of the measured differential magnitude vs. the actual differential magnitude. The solid line is for a separation of 1.″0, while the plus signs are for 0.″5. The standard deviation increases with increasing differential magnitude and decreasing separation.

much less scatter than from real binaries. Part of this scatter is explained by scintillation. Scintillation is a variance in the measured intensity from a given object. It arises when light rays traveling through regions of spatially and temporally varying refractive index changes are bent to form regions of relatively constructive and destructive interference at the telescope entrance pupil (Dravins et al. 1997).

The changes in the total intensity from a binary star are less than that from a single star, because the different stellar components see slightly different air paths and the combined variations tend to add less coherently than for a single source. The degree of incoherence increases with increasing separation. That is for the absolute photometry of both stars; scintillation also affects the differential photometry of the two components. Both absolute and differential scintillation decrease with wavelength, telescope aperture diameter, exposure time, and more benign atmospheric turbulence. Differential scintillation further depends on binary star separation and differential magnitude, as well as wind direction.

Ryan & Sandler (1998) studied differential scintillation using simulations of binary stars. Their simulations of a 2″ binary imaged by a 1.5 m telescope and a 6.5 m telescope showed an aperture dependency of $D^{-1.5}$, where D is the telescope diameter. This simulation used the Hufnagel-Valley atmospheric profile. Other atmospheric profiles would produce different results, since scintillation is dependent on the height of the turbulence. Differential scintillation is a small effect. For a 1.5 m telescope observing a 2″ binary at 800 nm with a 0.1 s exposure time the differential scintillation is 0.15%. This falls to 0.1% for a 0.25 s exposure. For a 6.5 m telescope the differential scintillation is approximately 0.02% for both exposure times (Ryan & Sandler 1998).

These results are only valid for the specified binary star observed with the specified observing conditions. Still they show that the 3.6 m AEOS telescope should be expected to have less differential scintillation than the SOR 1.5 m telescope; this is borne out in Figure 2 with the AEOS 700–1060 nm data having a lower scatter than the SOR *i*-band data.

2.2. *Anisoplanatism*

Another atmospheric property that will affect the measured differential magnitude is anisoplanatism, which causes spatially variant PSFs. This is because the farther light rays are from the optical axis, the less correlated the atmosphere they pass through is with the atmosphere encountered on-axis. The field of view over which the PSF is spatially correlated is called the isoplanatic patch, and the angle subtending it is the isoplanatic angle. In practice, the spatial correlation is found to fall off within a few arcseconds in the visible for uncorrected systems (Nisenson & Stachnik 1978; Schneiderman & Karo 1978). The decorrelation arises from differences in phase and in amplitude (i.e., scintillation), with the former being more significant (Yura & Fried 1998).

The ratio of the Strehl ratios of an off-axis source to an on-axis source is (Sasiela 1992)

$$\frac{S_{\rm off}}{S_{\rm on}} = e^{-(\theta/\theta_0)^5/3}, \quad (2)$$

where θ is the angular separation and θ_0 is the isoplanatic angle defined by

$$\theta_0 = \left[2.905\left(\frac{2\pi}{\lambda}\right)^2 \cos^{8/3}(\xi) \int_0^L C_n^2(z) z^{5/3}\, dz\right]^{-3/5}, \quad (3)$$

where ξ is the zenith angle, λ is the wavelength, z is the height, and C_n^2 is the atmospheric profile that gives the strength of the turbulence as a function of height (Fried 1982). It is important to note that this definition is only appropriate for uncorrected optical systems. If tip/tilt is corrected, the effective isoplanatic angle is larger (Fried 1976; Tyler 1984; Stone et al. 1994).

Analysis of the isoplanatic angle for AO systems leads to an apparent paradox. It would seem that for a star observed off-axis, the higher spatial (and temporal) frequency variations in phase should be increasingly less correlated with the on-axis variations. Correction of lower order modes would then leave the less spatially correlated higher order modes causing differences in the PSFs. One might then conclude that the isoplanatic angle was even less for a well-corrected system. Strictly speaking, this would be true, but in practice our ability to detect the differences in the PSFs diminishes as the order of the lowest uncorrected modes increases. In effect, we must remember that the isoplanatic angle of a measurement is not just that of the atmosphere but also includes the effect of the measuring system.

Since all real AO system are limited in their ability to respond to the strength and rapidity of atmospheric fluctuations, they are not able to achieve full correction. Also, since their correction changes from moment to moment, the effective isoplanatic angle changes on a similar timescale.

Exposure time is also a factor here. The longer the exposure time (which may be required due to poor AO performance as well as S/N), the more averaging of imperfections in the PSF will occur, which tends to make the PSFs look more alike and hence gives the impression of a larger isoplanatic angle (Bradford 1995).

Vertical distribution of the strength of turbulence is important, as can be seen by the altitude dependence in equation (3). This varies not only from site to site (Walters & Bradford 1997), but it also evolves over the course of the night (Avila et al. 2004). Different sites have stronger dominant layers and hence different isoplanatic angles.

Drummond et al. (2003) showed the effects of anisoplanatism in *I*-band images taken of the multiple star system ι Cas with the AEOS AO system. The A-B component had a separation of 2.″73 in 2001.565 and showed some anisoplanatism, although they were unable to quantify the anisoplanatism. The wider A-C component with a separation of 7.″29 understandably showed even more anisoplanatism, as the separation is outside the nominal *I*-band isoplanatic patch. The A-B component may or may not have been outside the patch.

Christou et al. (2003) showed that the effects of anisoplanatism can be seen in separations much less than the isoplanatic patch size. They presented *K*-band observations of binaries with separations of 11.″890 and 7.″623. The nominal isoplanatic patch size was computed to be 25″. These data were taken at Lick Observatory, which has a much lower altitude dominant turbulent layer than the Hawaiian observatories. These two case studies show that anisoplanatism does show up in binary stars with separations less than the nominal isoplanatic angle.

Even though most of the binary stars observed in the current study have separations less than the nominal isoplanatic patch, it is quite reasonable to assume that some of these binaries suffered from anisoplanatism and that this anisoplanatism changed between frames as the quality of the AO compensation changed and the atmospheric properties changed.

2.3. *Observing Recommendations*

Since we understand some of the causes of the frame-to-frame variability, we can take steps to minimize them. Some aspects of an observation are under the control of the observer and others

are not. The telescope aperture is not a free parameter in most observations. The wavelength is, but it is normally chosen for a specific science goal. The separation of the binary star is governed by the geometry of the system.

We can control the integration time and the number of data frames we collect. The effects of scintillation on binary stars go down as the integration time goes up. The S/N also increases with integration time, and this will enable the data analysis algorithm to produce a more accurate result. Longer integration times will average out fluctuations in the isoplanatic patch size, but this does not guarantee that the resulting PSFs are more accurate, merely that they have reached an average. Differences in the PSF caused by anisoplanatism will cause errors in astrometry and photometry in any technique that assumes a fixed PSF.

Co-adding data will minimize the frame-to-frame variability caused by scintillation. Co-adding 250 frames with individual exposure times of 0.1 s is effectively the same as taking a single integration of 25 s. Ryan & Sandler (1998) showed that the scintillation of a binary star with such a long integration time is negligible. This scenario is fairly typical of data collected on known binary stars with the AEOS AO system. For companion searches we normally collect 1000 frames, which allows us to probe a wider amount of dynamic range space by increasing S/N.

3. OBSERVATIONS

Observations of binary stars were made using the AEOS 3.6 m telescope and the AEOS AO system (Roberts & Neyman 2002) during 2002 and 2003. The AEOS AO is a natural guide star system using a Shack-Hartmann wavefront sensor. The individual subaperatures have a diameter of 11.9 cm projected onto the primary. The deformable mirror has 941 actuators. The system's closed loop bandwidth is adjustable and can run up to 200 Hz, although the normal range is approximately 50 Hz. The light from 500–540 nm is sent to the tip/tilt detector system, the light from 540–700 nm is sent to the wavefront sensor, and the light longer than 700 nm is sent to the Visible Imager CCD science camera or to other science instruments located in the observatory's coudé rooms.

In this paper, we present data sets taken with two different science instruments: the Visible Imager and the Kermit infrared camera (Perrin et al. 2003). The stars observed by both cameras were chosen to provide a range of binary separations between $0''$ and $5''$, as listed in the Washington Double Star Catalog (WDS; Mason et al. 2001), with a range of differential magnitudes. The Visible Imager data sets were taken with the Visible Imager on 2002 November 11, 2002 December 31, 2003 January 1, and 2003 January 3 UT. The Visible Imager has a Dove prism derotator, but it malfunctioned during the November 11 observing period and intermittently during the January 3 period. We do not report position angles when the derotator malfunctioned. In addition, all the reported astrometry was compared against the latest measurement listed in the WDS, and the reported values are consistent with the WDS measurements.

The Visible Imager data set consists of 250 frames taken on each binary star using a Bessel *I*-band filter. After collection, any saturated frames are discarded and the remaining frames are debiased, dark subtracted, and flat fielded. The frames are weighted by their peak pixel, which is proportional to their Strehl ratio and then co-added using a shift-and-add routine. The resulting image is analyzed with the program *fitstars*.

The second data set was taken in 2003 April with the Kermit infrared camera. The Kermit camera is a near-infrared camera using a Hawaii-2 2048×2048 detector. It is a reasonably fast readout, high dynamic range camera designed for *J*-, *H*-, and *K*-band observations. The camera was primarily built for the Lyot Project coronagraph (Oppenheimer et al. 2004), but it achieved first light during this experiment. Kermit was set up in one of the coudé rooms on the first floor of AEOS. The AO-compensated collimated beam was sent from the AO system into the coudé room where an off-axis parabolic mirror focused the beam onto the camera. No derotator or dispersion corrector was present. Between 50 and 100 frames were taken per object in each filter. The exceptions to this are STT 270, which only had 17 frames taken in *H*-band, and MCA 38, which had 122 frames taken in *H*-band as poor weather forced the closing of the telescope. Overall, the run suffered from bad weather and poor seeing.

The infrared camera Kermit was still undergoing development while these data were taken, and the data exhibit certain electrical artifacts, notably pickup of radio frequency interference (RFI) and ghost images of bright sources caused by cross talk between adjacent readout channels. These artifacts were removed in software. The RFI affected all readout channels identically, so the signal from an unilluminated channel provides a measure of the interference, which was subtracted from the illuminated channels. This step reduced the image rms background variance by an order of magnitude. Coefficients describing the cross talk between channels were obtained via least-squares fitting, and a suitably scaled and shifted version of the image was subtracted from the data to remove the cross talk. This cleaning process was largely cosmetic in nature; the cross talk artifacts were widely enough separated from the actual stellar images that they did not affect the photometry. The cleaned image was then flat-fielded, and bad pixels were interpolated across. After the above steps, the infrared data were co-added and analyzed in the same way as the Visible Imager data. As the infrared camera does not have an image derotator, we do not report position angles, and the pixel scale was not well known enough to produce accurate separations. Originally we had planned to observe many more stars, but poor weather and abysmal seeing limited our sample to those presented here.

4. RESULTS

In Table 2 we report 54 astrometric and photometric measurements of 39 multiple star systems taken in the *I* band. Table 3 lists photometric measurements of five binary stars with infrared *J*-, *H*-, and *K*-band filters.

Experience has shown that the *fitstars* reduction software measures separations accurate to 20% of a pixel when the PSFs are well separated; when the PSFs overlap, the accuracy decreases to 40% of a pixel. As the separation increases, anisoplanatism becomes more of an issue and the errors rise. Combining these factors with the error in determining the pixel yields the following error bars: $\pm 0\farcs02$ for separations less than $1''$, $\pm 0\farcs01$ for separations between $1''$ and $4''$, and $\pm 0\farcs02$ for separations greater than $4''$.

The derotator in the Visible Imager has two modes. The first mode mimics a camera mounted directly on the telescope. In this mode the zenith is always in the same position. The other mode is a standard astronomical mode, where north is fixed. We attempted to use the astronomical mode for all observations, but during some of the observations, the derotator mechanism malfunctioned and we were forced to use the zenith fixed mode. The error bar in the zenith fixed mode is $\pm 4^\circ$, while the error bar for the astronomical mode is $\pm 2^\circ$. This was determined by observing binaries with well-determined orbits[2] and comparing their computed position angles with the measured position angles.

[2] See http://ad.usno.navy.mil/wds/orb6/orb6c.html.

TABLE 2

PHOTOMETRY AND ASTROMETRY OF VISIBLE IMAGER DATA

WDS Number	Discovery Designation	*Hipparcos* Number	Besselian Year	ρ[a] (arcsec)	θ[b] (deg)	ΔI
02020+0246	STF 202 AB	9487	2002.8841	1.83	...	0.71 ± 0.03
03054+2515	STF 346 AB	14376	2002.8841	0.37	...	0.10 ± 0.03
03054+2515	STF 346 AC	14376	2002.8841	5.11	...	3.15 ± 0.01
03228+2045	HDS 423	15737	2002.8841	0.44	...	4.10 ± 0.14
03294+4931	BU 1179	16244	2002.8841	0.63	...	2.20 ± 0.03
04301+1538	STF 554	...	2002.9989	1.59	16	2.03 ± 0.01
04139+0916	BU 547 AB	19740	2002.8842	1.24	...	3.24 ± 0.06
04422+2257	MCA 16 Aa	21881	2002.8842	0.29	...	2.24 ± 0.03
			2002.9989	0.30	49	2.33 ± 0.03
04480+5645	HDS 617 Aa	22287	2003.0069	0.47	3	3.57 ± 0.09[c]
04593+3753	STF 616	23179	2002.8842	4.80	...	2.42 ± 0.01
05079+0830	STT 98	23879	2003.0069	0.79	314	0.82 ± 0.03
05081+2416	HDS 674 Aa	23900	2002.9989	0.38	202	3.11 ± 0.06
05293+2509	STF 716 AB	25695	2002.8842	4.67	...	0.90 ± 0.01
			2002.9990	4.66	207	1.06 ± 0.01
05293+2509	RBR 1 Aa	25695	2002.8842	1.79	...	6.1 ± 0.20[d]
			2002.9990	1.76	86	6.4 ± 0.20[c]
05293+2509	RBR 1 Ba	25695	2002.8842	0.97	...	3.28 ± 0.03[d]
			2002.9990	0.97	138	3.33 ± 0.03[c]
05308+0557	STF 728	25813	2002.8843	1.16	...	1.18 ± 0.01
05312+0318	STF 729 AB	36351	2002.8843	1.87	...	0.84 ± 0.01
			2003.0069	1.85	26	0.83 ± 0.01
05352+1014	STT 111	26215	2002.9990	2.76	351	4.55 ± 0.02
			2003.0070	2.76	351	4.23 ± 0.02
05413+1632	BU 1007	26777	2002.9990	0.25	237	1.49 ± 0.03
			2003.0070	0.26	239	1.46 ± 0.03
05472+1429	CHR 160	...	2002.9990	0.08	188	0.94 ± 0.05
05480+0627	STF 795	27386	2003.0070	1.08	216	0.41 ± 0.01
05500+0952	HEI 670	27549	2002.9990	1.02	265	3.14 ± 0.03
			2003.0071	1.00	260	3.03 ± 0.03
06041+2316	KUI 23 AB	28734	2002.9991	0.25	185	1.40 ± 0.05
			2003.0018	0.24	190	1.48 ± 0.05
			2003.0071	0.24	...	1.42 ± 0.05
06097+2307	BU 1241 AB	29225	2002.8818	0.61	...	2.91 ± 0.05
			2002.9991	0.60	345	2.80 ± 0.05
			2003.0018	0.61	346	2.80 ± 0.05
			2003.0071	0.60	...	2.85 ± 0.05
			2003.0071	0.60	...	2.85 ± 0.05
06379−1814	HDS 915	31700	2002.9991	1.10	2.9	5.08 ± 0.25
06564+0957	HDS 960	33372	2003.0076	0.74	207	2.99 ± 0.05[c]
07336+1550	MCA 32	36760	2002.9992	0.16	100	2.24 ± 0.05
07351+3058	STT 175 AB	36896	2002.9993	0.09	148	0.53 ± 0.03
08122+1739	STF 1196 AB	...	2002.9992	0.89	67	0.29 ± 0.03
			2003.0075	0.90	...	0.24 ± 0.01
09014+3215	STF 1298 AB	44307	2003.0076	4.43	134	2.37 ± 0.01
09077+1040	CHR 257	44798	2003.0077	0.30	104	3.23 ± 0.05
09285+0903	STF 1356	46454	2003.0077	0.61	89	0.67 ± 0.03
09521+5404	STT 208	48402	2003.0077	0.28	270	0.21 ± 0.05
10279+3642	HU 879	51233	2003.0077	0.22	216	2.06 ± 0.03
10350+0839	STF 1450	51802	2003.0077	2.13	156	1.94 ± 0.01
11182+3132	STF 1523	55203	2003.0077	1.79	256	0.59 ± 0.01
11159+1318	MCA 35	55016	2003.0077	0.12	139	1.13 ± 0.05
11239+1032	STF 1536 AB	55642	2003.0078	1.78	303	2.41 ± 0.01
11479+0815	RBR 2 Aa-b	57562	2003.0078	2.90	173	7.9 ± 0.40[d]

[a] The error bar is $\pm 0''.02$ for $\rho \leq 1''$, $\pm 0''.01$ for $1'' < \rho \leq 4''$, and $\pm 0''.02$ for $\rho > 4''$.

[b] The position angles all have an error bar of $\pm 2^{\circ}$.

[c] Confirmation observation.

[d] New discovery.

TABLE 3
PHOTOMETRY OF KERMIT DATA

WDS Number	Discovery Designation	*Hipparcos* Number	Besselian Year	ΔJ	ΔH	ΔK
10350+0839	STF 1450	51802	2003.2952	1.99 ± 0.01	2.04 ± 0.01	2.13 ± 0.01
11479+0815	RBR 2 Aa-b	57562	2003.2953	7.9 ± 0.3	6.9 ± 0.3	6.7 ± 0.3
11486+1417	BU 603	57606	2003.2954	2.07 ± 0.01	1.84 ± 0.01	1.73 ± 0.01
13099−0532	MCA 38 Aa	64238	2003.2955	2.65 ± 0.03	2.50 ± 0.03	2.56 ± 0.03
13473+1727	STT 270	67275	2003.2955	...	4.08 ± 0.05	...

The photometry error bars for co-added visible data were generated in a similar manner to the ones for single frames in Figure 4. The error curves depend on whether the companion is located on top of the PSF halo or not. Only relatively bright companions are found in the halo, as the halo overwhelms faint companions. In addition, the halo increases the photometric error for companions located inside of it. For the infrared data, we used the last reported separation value listed in the WDS in place of the measured separation.

As a check on the accuracy of our astrometry, we compared our measurements with the predicted positions for those systems that have orbits computed. These systems are listed in Table 4. The standard deviation of the observed minus computed ($O-C$) separation is 0.″029 and 4.°7 for the position angle. This is a combination of errors in our measurements and errors in the computed orbits. WDS 03054+2515, WDS 04301+1538, WDS 05079+0830, and WDS 05308+0557 all had $O-C$ separation differences larger than 1 σ from zero. These are graded 3, 4, 3, and 4, respectively, by the Sixth Catalog of Orbits of Visual Binary Stars.[3] WDS 05413+1632, WDS 06041+2316, and WDS 07351+3058 had position angles greater than 1 σ from zero. WDS 06041+2316 has two measurements, one of which is very close to the computed value, and we assume the second measurement was a bad measurement. The other two systems have orbits that are graded 3. Since none of the stars have $O-C$ larger than 1 σ from zero in both position angle and separation, this suggests that none of the orbits are dramatically incorrect.

We made observations that confirmed the multiplicity of WDS 04480+5645 (HDS 617 Aa) and of WDS 06564+0957 (HDS 960). Both confirmation observations are consistent with the discovery observations.

Three of the binaries we observed were also observed by ten Brummelaar et al. (2000) with the natural guide star AO system on the Hooker 100 inch telescope at Mount Wilson. Both sets of observations used the same data reduction technique, but having common targets allows us to determine whether there are any systematic errors caused by the different AO systems. For WDS 04139+0916, ten Brummelaar et al. (1998) reported a ΔI of 3.28 ± 0.13. We report a ΔI of 3.24 ± 0.06. Both measurements are within the error bars. We also have excellent agreement for WDS 05413+1632, for which ten Brummelaar et al. reported a ΔI of 1.52 ± 0.18 and we report two measurements of ΔI: 1.49 ± 0.03 and 1.46 ± 0.03.

The agreement is not as good for WDS 11182+3132, for which ten Brummelaar et al. (1998) reported ΔI measurements of 0.40 ± 0.04 and 0.18 ± 0.04, while we report a ΔI of 0.59 ± 0.01. It is significant that the ten Brummelaar et al. measurements do not agree with themselves, indicating the possibility of either an error with those measurements or short-term variability of one of the stars, possibly an eclipsing binary. The AEOS observation shows two well-separated stars with very low differential magnitude. This is ideal for very small errors (see § 2). We do not have a satisfactory explanation for the spread in the measurements; we will continue to monitor the object to see whether the answers converge. The agreement between most of the current measurements and the ten Brummelaar et al. measurements shows that there is nothing systematic in either AO system that biases the results.

4.1. *New Companions*

In the course of these observations, we detected three new companions to two previously known multiple star systems. The WDS numbers, assigned discovery designations, and Besselian dates of discovery are listed in Table 5, while the astrometry and photometry are listed in Tables 2 and 3.

We were observing WDS 05293+2509 (STF 716 AB) when we detected fainter companions to each of the two components. The two new pairs were designated RBR 1 Aa and RBR 1 Ba. The discovery was confirmed a few weeks later, and both measurements are listed in Table 2. Based on the absolute magnitude for MK dwarfs listed in Cox (2000) and the B8.5 V spectral type

[3] The Sixth Catalog of Orbits of Visual Binary Stars is located at http://ad.usno.navy.mil/wds/orb6.html.

TABLE 4
RESOLVED STARS WITH COMPUTED ORBITS

WDS	References
02020+0246	Scardia (1983)
03054+2515	Heintz (1981)
04301+1538	Baize (1980)
05079+0830	Baize (1969)
05308+0557	Seymour & Hartkopf (1999)
05413+1632	Docobo & Ling (1999)
06041+2316	Heintz (1986)
07351+3058	Hartkopf et al. (1989)
08122+1739	Soderhjelm (1999)
09285+0903	van Dessel (1976)
09521+5404	Heintz (1996)
10279+3642	Mason & Hartkopf (2001)
11182+3132	Mason et al. (1995)
11239+1032	Soderhjelm (1999)

TABLE 5
NEW COMPANIONS

WDS Number	Discovery Designation	*Hipparcos* Number	Besselian Year
05293+2509	RBR 1 Aa	25695	2002.8842
05293+2509	RBR 1 Ba	25695	2002.8842
11479+0815	RBR 2 Aa-b	57562	2003.0078

TABLE 6
MAGNITUDES OF INDIVIDUAL COMPONENTS

WDS Number	Discovery Designation	J_1 (mag)	J_2 (mag)	H_1 (mag)	H_2 (mag)	K_1 (mag)	K_2 (mag)
10350+0839	STF 1450 AB	5.67 ± 0.03	7.66 ± 0.03	5.66 ± 0.03	7.70 ± 0.03	5.58 ± 0.02	7.71 ± 0.02
11479+0815	RBR 2 Aa-b	5.27 ± 0.02	13.2 ± 0.2	5.30 ± 0.04	12.20 ± 0.17	5.25 ± 0.02	12.0 ± 0.16
11486+1417	BU 603	5.42 ± 0.02	7.49 ± 0.02	5.35 ± 0.02	7.19 ± 0.02	5.32 ± 0.02	7.05 ± 0.02
13099−0532	MCA 38	4.62 ± 0.28	7.27 ± 0.28	4.66 ± 0.08	7.16 ± 0.08	4.49 ± 0.04	7.05 ± 0.04

of the combined system (Walter & Boyd 1991), we computed rough spectral types for the components of WDS 045293+2509. Our results indicate that the previously known A and B components have spectral types of B9 and early A, respectively, while the new companion to A has a spectral type somewhere between K6 and K9 and the new companion to B is roughly a G5 star. This analysis assumed the stars are all on the main sequence and form a physical system. We are unable to determine whether the system is bound with observations in a single color at a single epoch,but the companions do appear to form hierarchal systems. The system will continue to be monitored to see whether we can detect orbital motion.

While observing WDS 11479+0815 (CHR 134 Aa), we detected a companion almost 3″ from the main system with a ΔI of 7.9 ± 0.4. The companion was confirmed with the Kermit camera observations in 2003 April, and the pair was given the discovery designation RBR 2 Aa-B. While the companion is several arcseconds from the primary, it has a smaller separation than the other components of the system, SHJ 131 Aa-B and SHJ 131 Aa-C. None of our observations resolved the inner CHR 134 Aa component, but it is doubtful that this component, which had a 1987 separation of 0.″3, would have moved to 2.″9. Also, the measured differential magnitude of 7.9 in the *I* band would have been far too large for the CHARA speckle camera to detect (Mason 1994).

From both the Visible Imager and the Kermit data we have *I*, *J*, *H*, and *K* differential magnitudes. The 2MASS Catalog[4] lists the total *J*, *H*, and *K* magnitudes for this system as 5.27 ± 0.023, 5.30 ± 0.038, and 5.25 ± 0.017, respectively. Combining these with the differential magnitudes we are able to compute the *J*, *H*, and *K* magnitudes for the CHR 134 Aa pair, as well as the newly discovered star. These are listed in Table 6. We are unable to do this for the *I*-band measurement, because we do not have an *I*-band measurement for the entire system.

The component has a fairly high dynamic range, and the error bar on the determined magnitudes are high. This error causes a great deal of uncertainty in the derived spectral type. The computed colors are very red. Further observations are necessary to determine whether it is a late-type star or a background object.

4.2. *Spectral Typing*

There are three stars with differential magnitudes measured in multiple filters, which allows us to analyze the spectral types of these stars. They are WDS 10350+0839 (STF 1450), WDS 11486+1417 (BU 603), and WDS 13099-0532 (MCA 38). Using 2MASS *J*, *H*, and *K* magnitudes of the entire system we computed individual magnitudes of each component; these are listed in Table 6. From these we can compute colors for each star in the system. In general, we found the $(J-K)$ and $(J-H)$ colors to be more useful than the $(H-K)$ colors. The $(H-K)$ colors are very small and the error bars tend to be larger than these differences, rendering that color insensitive to different spectral types.

Cowley et al. (1969) gives a spectral type for the entire STF 1450 system of A2 V. The primary colors that we measure are $(J-K) = 0.09 \pm 0.036$ and $(J-H) = 0.01 \pm 0.04$, which indicates an early A star. The secondary colors are $(J-K) = -0.05 \pm 0.04$ and $(J-H) = -0.04 \pm 0.04$, which matches a late B star. This is quite odd, as the secondary's colors are bluer than the primary's. Chambliss (1992) lists one of the components as being an eclipsing Algol-type binary with a 2.455 day period. If the eclipsing component were the primary, it would redden the component and possibly make it appear redder than the secondary.

The picture is clearer for BU 603. The colors from the primary yield a spectral type of late A to early F, while the secondary is a late F to a late G star. This agrees with Edwards (1976), who determined the spectral types of A8 V and G2 V. His determination does not have a formal error, but he notes that errors are normally only ±2–3 subclasses. Heintz (1991) gives a mass fraction of 0.396, which is consistent with the determined spectral types. While we are unable to expand on Edward's earlier work, the agreement between the two is reassuring and lends credibility to our analysis of other systems.

We are unable to determine the spectral type with the MCA 38 data, because the 2MASS *J* magnitude has a much larger error than normal. All the other magnitudes had errors on the order of a few percent, while the MCA 38 *J* error bar was ±0.282. This error propagates into the color errors and renders spectral typing useless.

4.3. *Unresolved Binaries*

Not all of the binary stars that were observed were resolved. Table 7 lists 23 unresolved systems. The table gives the WDS number, the discovery designation, the *Hipparcos* number, the Besselian date of observation, and the FWHM of the co-added image for each binary. The FWHM provides a rough idea to what separation we could have resolved. It is not a perfect correspondence, since resolving companions is also dependent on the differential magnitude of the system: the brighter the companion, the easier it is to separate. The FWHM varies with AO performance, which is dependent on the brightness of the star, elevation angle, and atmospheric conditions; as such, it fluctuates from star to star. The FWHM should be useful as a check in later orbit determination. As a check on orbit quality, we compared the measured FWHM with the predicted separation for those systems with orbits; in all cases the FWHM was larger.

For most stars the FWHM is close to the last measured separation, and it is assumed that the binary is lost in the PSF. In two cases we failed to detect systems that we should have been able to detect. We were unable to resolve the HEI 202 Aa component of WDS 00484+0517; the wider BUP 10 Aa-B component had a 1929 separation of 181.″2, and we would not expect to detect that. The WDS lists the HEI 202 Aa pair as having two

[4] Information about the 2MASS All-Sky Data Release can be found at http://www.ipac.caltech.edu/2mass/releases/allsky.

TABLE 7
Unresolved Binary Stars

WDS Number	Discovery Designation	*Hipparcos* Number	Besselian Year	FWHM (arcsec)
02424+2001	BLA 1 Aa	12640	2003.0069	0.10
00484+0517	HEI 202 Aa	3765	2003.0069	0.08
04044+2406	MCA 13	19009	2002.8842	0.14
04053+2201	CHR 158 Aa	19076	2002.8842	0.12
04184+2135	MCA 14 Aa	20087	2002.8842	0.14
04235+2059	CHR 16	20493	2002.8841	0.12
04493+3235	CHR 19	22407	2002.8842	0.12
05074+1839	A 3010	23835	2002.8843	0.14
			2002.9989	0.14
05134+3829	CHR 256	12704	2002.8843	0.17
05272+1758	MCA 19 Aa	25499	2002.8843	0.12
			2002.9990	0.14
			2003.0017	0.13
05348+0929	MCA 20	26176	2002.9990	0.12
			2003.0070	0.12
05490+2434	HDS 782 AC	27468	2003.0071	0.10
05490+2434	MCA 23 AB	27468	2003.0070	0.09
06035+1941	MCA 24	28691	2002.9990	0.13
			2003.0018	0.16
06290+2013	BTZ 1 Aa	30883	2002.9991	0.13
			2003.0018	0.14
			2003.0075	0.08
06120+1947	CHR 163	29433	2003.0018	0.13
07134+1610	HDS 1003 Aa	34909	2002.9992	0.10
07269+2015	CHR 26	36156	2002.9992	0.12
07277+2127	MCA 30 Aa	36238	2002.9992	0.12
07298+2755	MCA 31 Aa	36429	2002.9993	0.09
11006+0337	CHR 33	53807	2003.0077	0.10
11191+3811	CHR 133	55266	2003.0077	0.14
11416+3145	BNU 3 Aa	57029	2003.0078	0.10

measurements, both with a separation of 2.″7. The FWHM of the image was 0.″08, which shows the AO system was working exceptionally well. We could be expected to see any binaries with a separation greater than this if the magnitudes were close. As the separation increases we would have been able to see higher dynamic range systems. Our image had a wide enough field of view that any binary within 4.″2 would have been detectable; while the field of view of the camera is 10″, the star was not centered in the image. The S/N of the image was high enough that we would have been able to detect at the 3 σ level a binary star with a dynamic range of less than 10 mag, based on a comparison of the peak of the image to the background noise.

Heintz & Borgman (1984) were able to detect the companion twice, but they were unable to detect it on an additional 169 plates and with visual use of a micrometer. During the two positive detections, the differential magnitude varied. Heintz and Borgman concluded that the companion was a flare star. HEI 202 Aa was discovered photographically, which is more sensitive in the blue than in the red. It is possible that the unseen companion is blue enough that it exceeds the dynamic range limit of the AO *I*-band observations. Since the composite spectral type of HEI 202 Aa is K2 V (Cowley et al. 1967), the companion would have to be a white dwarf to escape detection, which is inconsistent with Heintz and Borgman's conclusion that the star was a flare star.

We also did not resolve any of the components of WDS 05490+2434. The MCA 23 AB pair has a single measurement of 0.″043 in 1978 (McAlister & Hendry 1982). Mason et al. (1999) published 22 negative detections of this system. The single measured separation is small enough that we would not expect to see it with the AEOS AO system. What is surprising is that we did not resolve the wider HDS 782 AC system with two 1991 measurements with listed separations of 3.″77 as reported by *Hipparcos* (Perryman et al. 1997) and Fabricius et al. (2002). The Mason et al. observations would not have seen this companion, because their field of view was too small. The FWHM of our image was 0.″09, and the field of view was 4.″7. No companions were detected in this range. The S/N of the image is high enough that we would have been able to detect at the 3 σ level a binary star with a dynamic range of less than 9 mag, based on a comparison of the peak of the image to the background noise.

5. SUMMARY

We used the AEOS AO system to observe numerous binary stars and report astrometry and photometry for 39 systems. We were unable to resolve an additional 23 systems, in most cases because the separations were too small. During the course of this study we discovered two additional possible components to the WDS 05293+2509 system and another possible companion in the WDS 11479+0815 system. We also analyzed the various factors that have an impact on the errors in the determination of differential magnitudes in AO images. The effects of scintillation an anisoplanatism can be minimized for a given telescope by taking either longer exposures or many shorter exposures and co-adding them.

We thank Brian Mason and Bill Hartkopf for providing data from the Washington Double Star Catalog (WDS) and for useful

and insightful comments. Also, we thank the numerous staff members of the Maui Space Surveillance System who helped make this data possible. This research was funded by the Air Force Office of Scientific Research through AFRL/DE (contract F29601-00-D-0204) and by the National Science Foundation (NSF) through grants AST 00-88316 and AST 02-15793. B. R. O. was partially supported by the American Museum of Natural History's Kalbfleisch Fund. T. A. t. B. was supported by the Center for High Angular Resolution Astronomy at Georgia State University. M. D. P. was supported by a NASA Michelson Graduate Fellowship under contract to the Jet Propulsion Laboratory funded by NASA. This research made use of the WDS maintained at the US Naval Observatory, the SIMBAD database, operated by the CDS in Strasbourg, France, and data products from the Two Micron All Sky survey, which is a joint project of the University of Massachusetts and the Infrared Processing and Analysis Center, California Institute of Technology, funded by NASA and the NSF.

REFERENCES

Avila, R., Masciadri, E., Vernin, J., & Sánchez, L. J. 2004, PASP, 116, 682
Baize, P. 1969, IAU Comm. 26 Inf. Circ., 48, 1
———. 1980, A&AS, 39, 83
Barnaby, D., Spillar, E., Christou, J. C., & Drummond, J. D. 2000, AJ, 119, 378
Bradford, L. W. 1995, Ph.D. thesis, Univ. California, Santa Cruz
Chambliss, C. R. 1992, PASP, 104, 663
Christou, J. C., Pugliese, G., Köhler, R., & Drummond, J. D. 2004, PASP, 116, 734
Christou, J. C., Steinbring, E., Faber, S. M., Gavel, D., Patience, J., & Gates, E. 2003, Proc. SPIE, 4839, 846
Cowley, A., Cowley, C., Jaschek, M., & Jaschek, C. 1969, AJ, 74, 375
Cowley, A. P., Hiltner, W. A., & Witt, A. N. 1967, AJ, 72, 1334
Cox, A. N. 2000, Allen's Astrophysical Quantities (New York: Springer)
Docobo, J. A., & Ling, J. F. 1999, ApJS, 120, 41
Dravins, D., Lennart, L., Mezey, E., & Young, A. T. 1997, PASP, 109, 173
Drummond, J., Milster, S., Ryan, P., & Roberts, L. C., Jr. 2003, ApJ, 585, 1007
Edwards, T. 1976, AJ, 81, 245
Esslinger, O., & Edmunds, M. G. 1998, A&AS, 129, 617
Fabricius, C., Hög, E., Makarov, V. V., Mason, B. D., Wycoff, G. L., & Urban, S. E. 2002, A&A, 384, 180
Fried, D. L. 1976, Proc. SPIE, 75, 20
———. 1982, J. Opt. Soc. Am., 72, 52
Fugate, R. Q., et al. 1994, J. Opt. Soc. Am. A, 11, 310
Hartkopf, W. I., McAlister, H. A., & Franz, O. G. 1989, AJ, 98, 1014
Heintz, W. D. 1981, ApJS, 45, 559
———. 1986, A&AS, 65, 411
———. 1991, AJ, 101, 1071
———. 1996, AJ, 111, 412
Heintz, W. D., & Borgman, E. R. 1984, AJ, 89, 1068
Mason, B. D. 1994, Ph.D. thesis, Georgia State Univ.
Mason, B. D., & Hartkopf, W. I. 2001, IAU Comm. 26 Inf. Circ., 144, 1
Mason, B. D., McAlister, H. A., Hartkopf, W. I., & Shara, M. M. 1995, AJ, 109, 332
Mason, B. D., Wycoff, G. L., Hartkopf, W. I., Douglass, G. G., & Worley, C. E. 2001, AJ, 122, 3466
Mason, B. D., et al. 1999, AJ, 117, 1890
McAlister, H. A., & Hendry, E. M. 1982, ApJS, 49, 267
Nisenson, P., & Stachnik, R. V. 1978, J. Opt. Soc. Am., 68, 169
Oppenheimer, B. R., et al. 2004, Proc. SPIE, 5490, 433
Perrin, M. D., Graham, J. R., Trumpis, M., Kuhn, J., Whitman, K., Coulter, R., Lloyd, J. P., & Roberts, L. C., Jr. 2003, in Proc. 2003 AMOS Conf. (CD-ROM; Kihei: Maui Economic Dev. Board)
Perryman, M. A. C., et al. 1997, The *Hipparcos* and Tycho Catalogs (ESA SP-1200; Noordwijk: ESA)
Roberts, L. C., Jr. 1998, Ph.D. thesis, Georgia State Univ.
Roberts, L. C., Jr., & Neyman, C. R. 2002, PASP, 114, 1260
Ryan, P., & Sandler, D. 1998, PASP, 110, 1235
Sasiela, R. J. 1992, J. Opt. Soc. Am. A, 9, 1398
Scardia, M. 1983, Astron. Nachr., 304, 257
Schneiderman, A. M., & Karo, D. P. 1978, J. Opt. Soc. Am., 68, 338
Seymour, D., & Hartkopf, W. 1999, IAU Comm. 26 Inf. Circ., 139, 2
Shelton, J. C., Schneider, T., McKenna, D., & Baliunas, S. L. 1995, Proc. SPIE, 2534, 72
Soderhjelm, S. 1999, A&A, 341, 121
Stone, J. P., Hu, P. H., Mills, S. P., & Ma, S. 1994, J. Opt. Soc. Am. A, 11, 347
Strehl, K. 1901, Z. Instrum., 22, 213
ten Brummelaar, T. A., Hartkopf, W. I., McAlister, H. A., Mason, B. D., Roberts, L. C., Jr., & Turner, N. H. 1998, Proc. SPIE, 3353, 391
ten Brummelaar, T. A., Mason, B. D., Bagnuolo, W. G., Jr., Hartkopf, W. I., McAlister, H. A., & Turner, N. H. 1996, AJ, 112, 1180
ten Brummelaar, T. A., Mason, B. D., McAlister, H. A., Roberts, L. C., Jr., Turner, N. H., Hartkopf, W. I., & Bagnuolo, W. G., Jr. 2000, AJ, 119, 2403
Tyler, G. A. 1984, J. Opt. Soc. Am. A, 1, 251
van Dessel, E. 1976, A&AS, 26, 415
Walter, F. M., & Boyd, W. T. 1991, ApJ, 370, 318
Walters, D. L., & Bradford, W. L. 1997, Appl. Opt., 36, 7876
Yura, H. T., & Fried, D. L. 1998, J. Opt. Soc. Am. A, 15, 2107